Damage Tolerance of a Hanging Clothes Bag

[redacted]
Wichita State University, Wichita, Kansas, 67260

An investigation into the damage tolerance of a hanging clothes bag is presented. The purpose of the investigation has been to discover the cause of the internal support structure failing under repeated use. Failure analysis has been accomplished through the study of the stress intensity, residual strength, fatigue life, and crack propagation. It has been shown that the support structure fails due to fracture at short crack lengths, but transitions to failure due to net-section yielding at longer crack lengths. Additionally, recommendations for proper inspection intervals and damage-tolerant improvements have been provided.

Nomenclature

K_I	=	mode I stress intensity, psi*(in)$^{1/2}$
σ	=	applied remote stress, psi
c	=	crack length, in
r_p	=	plastic zone radius, in
I	=	plane stress/strain conversion factor
c_{eff}	=	effective crack length, in
β	=	shape factor
σ_{br}	=	rivet bearing stress, psi
P_r	=	rivet load, lb/in
R	=	rivet hole radius, in
w	=	panel width, in
D	=	rivet hole diameter, in
t	=	panel thickness, in
b	=	stiffener spacing, in
P_s	=	rivet spacing, in
μ	=	panel-comparison factor
A_s	=	cross-sectional area of stiffener, in^2
E_s	=	Young's Modulus of stiffener, psi
A	=	cross-sectional area of skin, in^2
E	=	Young's Modulus of skin, psi
K_{Ic}	=	fracture toughness, psi*(in)$^{1/2}$
σ_c	=	critical strength, psi
σ_{YS}	=	yield strength, psi
B_f	=	blocks to failure
σ_r	=	residual strength, psi
N_j	=	cycles of current load
N_{fj}	=	cycles to failure of current load
σ_a	=	stress amplitude, psi
σ_m	=	mean stress, psi
σ_f'	=	material constant, psi
b	=	material constant
ϵ_a	=	total strain amplitude
ϵ_e	=	elastic strain amplitude
ϵ_p	=	plastic strain amplitude
c_2	=	material constant
ϵ_f'	=	material constant
S	=	Walker-Boeing load, psi
p	=	Walker-Boeing material constant
q	=	Walker-Boeing material constant
Z	=	Walker-Boeing scale factor
R_2	=	stress ratio
c_0	=	initial crack length, in
c_f	=	final crack length, in
C	=	Paris law constant
n	=	Paris law constant
m_T	=	Walker-Boeing material constant

I. Introduction

Hanging clothes bags are typically not in the forefront of an individual's mind. However, for the frequent traveler, such as a corporate CEO or an esteemed professor presenting research on fracture mechanics, a functioning clothes bag is vital to keeping suits wrinkle-free. On the rare occasion that the internal support structure of one of these bags fails, an audience's attention to one's presentation could be shifted toward wrinkles on one's lapel.

On a recent trip to a wedding, the internal support of a student's clothes bag failed due to cracking around a rivet hole, as shown in fig. 1. An investigation into the cause of the failure was initiated, which included a study of the

* Graduate Student, Department of Aerospace Engineering, 1845 Fairmount Street, Box 44, Wichita, KS, 67260-0044.

stress intensity, residual strength, fatigue life, and crack propagation. Additionally, inspection intervals and possible damage-tolerant improvements were investigated.

To accomplish this, the structure was approximated as a finite-width, stiffened panel, with symmetric edge-cracks around a centered hole, a remoted stress, and a fastener load. A diagram of the panel is shown in fig. 2. Additionally, the loads and material properties of the plastic were estimated as shown in table 1.

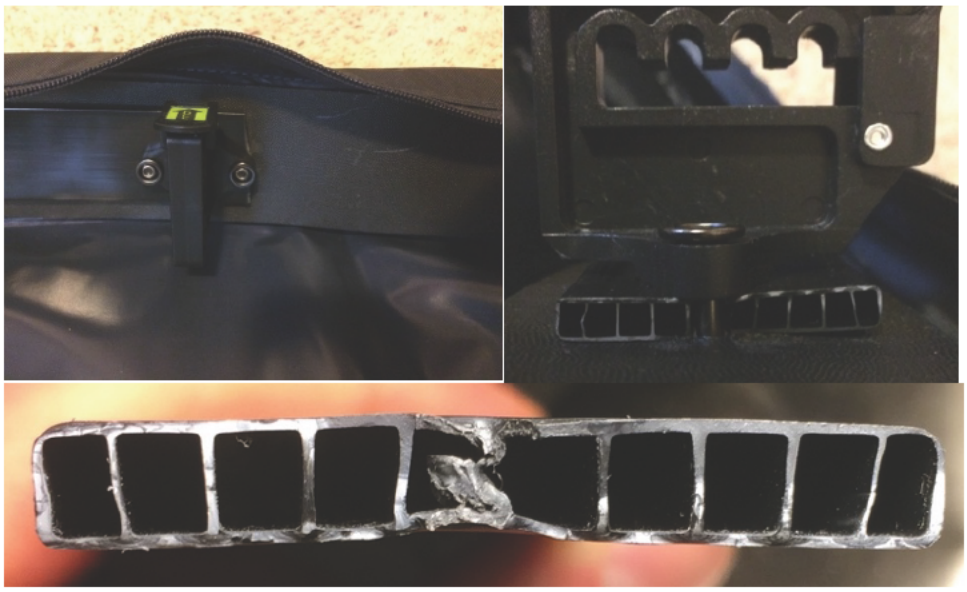

Figure 1. Failure of the support structure at the rivet hole.

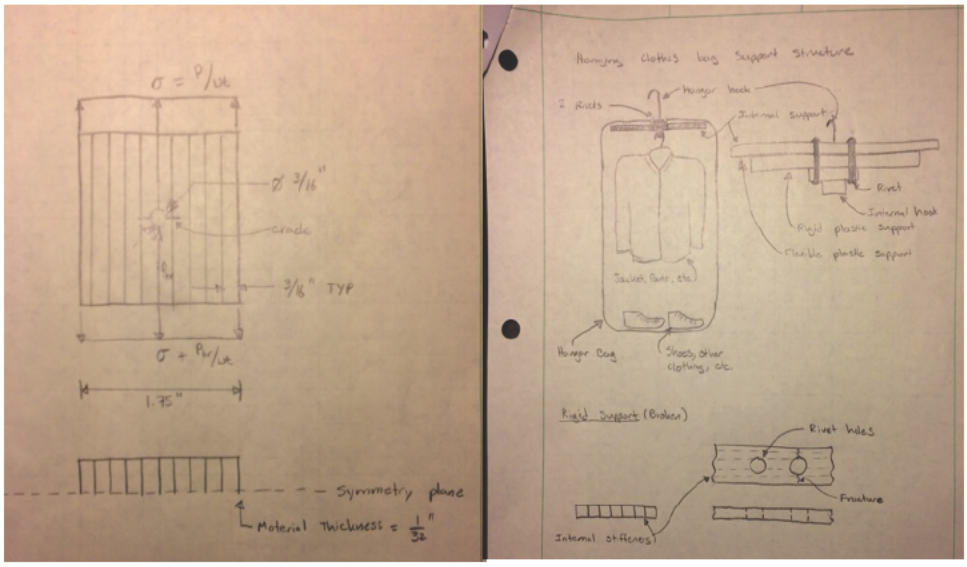

Figure 2. Schematic of the Panel. *The schematic shows the panel and the configuration within the support structure.*

Table 1. Panel Properties.

Category	Item	Original Panel (plastic)	Improved Panel (Aluminum 2024-T351)	Unit
Panel Dimensions	Hole Diameter, D	0.1875	0.1875	in
	Panel Width, w	1.75	1.75	in
	Panel Thickness, t	0.03125	0.0625	in
	Stiffener Spacing, b	0.1875	0.1875	in
	Stiffener Width, w2	0.25	0.25	in
	Stiffener thickness, t2	0.03125	0.0625	in
Panel Loads	Remote Stress, sigma	2	2	psi
	Fastener Load, P_r	1	1	lb/in
Material Properties	Yield Stress, sigma_ys	32	55000	psi
	Fracture Toughness, K_c	6	32000	psi(in)^(1/2)
	Stiffener Yield Stress, sigma_ys2	32	55000	psi
	Skin Young's Modulus, E	560	1.06E+07	psi
	Stiffener Young's Modulus, E_s	560	1.06E+07	psi
Fatigue Properties	(sigma_f)'	25	134000	psi
	b	-0.102	-0.113	-
	c	-0.743	-0.713	-
	(epsilon_f)'	0.4	0.409	-
	q	0.6	0.6	-
	p	3.5	3.9	-
Crack Propagation Properties	Paris Law C	6.75E-04	6.75E-10	-
	n	3.89	3.89	-
	M_t	0.6	1.26	-

II. Stress Intensity

Stress intensity is a measure of the local magnitude of stress, namely the magnitude at the tip of a crack. This is used to compare the relative severity of one crack to another. For the support structure, the stress intensity was calculated both with and without the stiffeners included, in order to investigate the effect of the stiffeners. Additionally, the plastic-stress-intensity ratio was calculated to study the effects of plasticity in the structure.

A. Stress Intensity

The stress intensity was calculated for an unstiffened panel, as well as for a stiffened panel, so that the results could be compared. This was accomplished according to Eq. (1). In both cases, the effect of plasticity in the material was included by computing an effective crack length in accordance with equations (2) – (4).

$$K_I \quad \sigma\sqrt{\pi c_{eff}}\beta \tag{1}$$

$$r_p \quad \frac{1}{I\pi}\left[\frac{K_I}{\sigma_{YS}}\right]^2 \tag{2}$$

$$I \quad \begin{cases} 2 & if\ I \le 2 \\ 6.7 \quad \frac{1.5}{t}\left[\frac{K_I}{\sigma_{YS}}\right]^2 & if\ 2 < I < 6 \\ 6 & if\ I \ge 6 \end{cases} \tag{3}$$

$$c_{eff} \quad \boldsymbol{c + r_p} \tag{4}$$

For each case, the shape factor, β, was calculated in a slightly different manner, which is described in the following subsection. However, the results of the calculation showed that the presence of stiffeners greatly reduced the stress intensity, as shown in fig. 3. For the unstiffened panel, the stress intensity tended to continually increase as the crack

length increased. However, the stiffened panel tended to remain within the range of 0.5 psi(in)$^{1/2}$ to 1 psi(in)$^{1/2}$, with the low points corresponding to the location of the stiffeners.

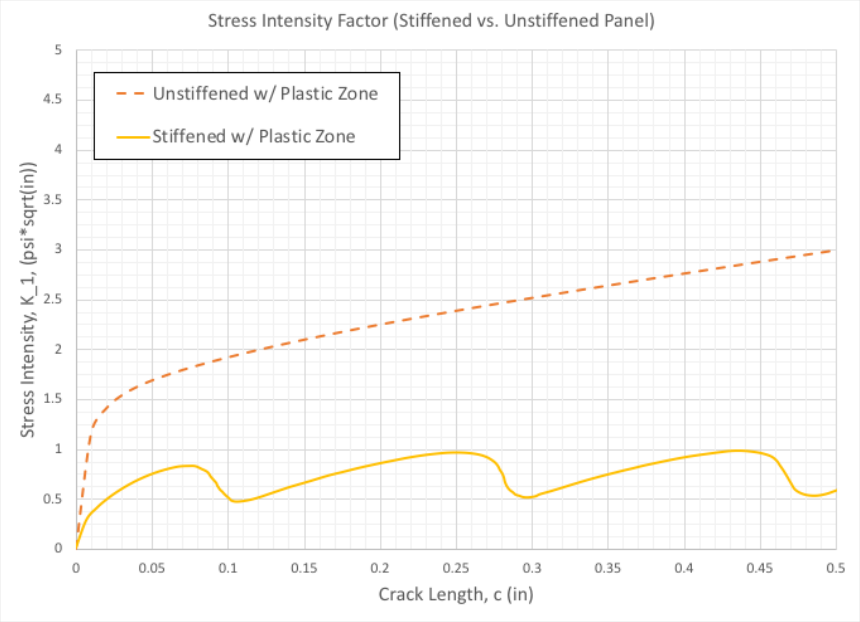

Figure 3. Stress Intensity Factor. *The graph above shows the effect of stiffeners on the stress intensity factor as a function of crack length.*

B. Stress Intensity Shape Factor, β

For the case of the unstiffened panel, the shape factor, β, was calculated according to equations (5) – (10).

$$\beta \quad F_{c/R}F_wF_{ww} + \frac{\sigma_{br}}{\sigma}F_3F_wF_{ww} \tag{5}$$

$$F_{c/R} \quad \left(3.4040 + 3.1872\left(\frac{c}{R}\right)\right) / \left(1 + 3.9273\left(\frac{c}{R}\right) \quad 0.00695\left(\frac{c}{R}\right)^2\right) \tag{6}$$

$$F_w \quad \sqrt{\sec\left(\frac{\pi R}{w}\right)\sec\left(\frac{\pi(R+c)}{w}\right)} \tag{7}$$

$$F_{ww} \quad 1 \quad \left(\left(\frac{1.32w}{D} \quad 0.14\right)^{\left(0.98+\left(\frac{0.\ w}{D}\right)^{0.}\right)} \quad 0.02\right)\left(\frac{2c}{w\ \ D}\right)^{\frac{w}{D}\ 2.5} \tag{8}$$

$$F_3 \quad 0.98 + 0.3592\boldsymbol{e}^{\frac{-3.5089c}{R}} + 0.3817\boldsymbol{e}^{\frac{-0.551c}{R}} \tag{9}$$

$$\sigma_{br} \quad \frac{P_r}{Dt} \tag{10}$$

In the case of the stiffened panel, the shape factor was taken from experimental data for a crack centered between stiffeners. Since the experimental data was provided for limited cases, depending on rivet pitch and the panel-comparison factor, some assumptions were necessary in order to use this data. Rivet pitch is the ratio of the rivet spacing on a stiffener to the spacing of the stiffeners themselves, as shown by Eq. (11).

$$Rivet\ Pitch \quad \frac{P_s}{b} \tag{11}$$

As the rivet spacing decreases, this ratio approaches zero. In the case of the panel of interest, the stiffeners are an integral part of the panel, effectively requiring the rivet spacing, and thus the rivet pitch to be zero. The smallest rivet pitch within the data available is 1/12. This data was assumed to closely approximate a rivet pitch of zero and was used to model the shape factor for the stiffened panel and stiffeners.

Additionally, the panel-comparison factor, μ, was calculated according to Eq. (12).

$$\mu \quad \frac{A_S E_S}{A_S E_S + AE} \tag{12}$$

For the panel of interest, the panel-comparison factor was computed to be $\mu = 0.125$. The chart for $\mu = 0.3$ was assumed to be a close approximation and was used for the calculation of the shape factor. Figure 4 shows the shape factor as a function of the crack length for the unstiffened panel, stiffened panel, and the stiffener.

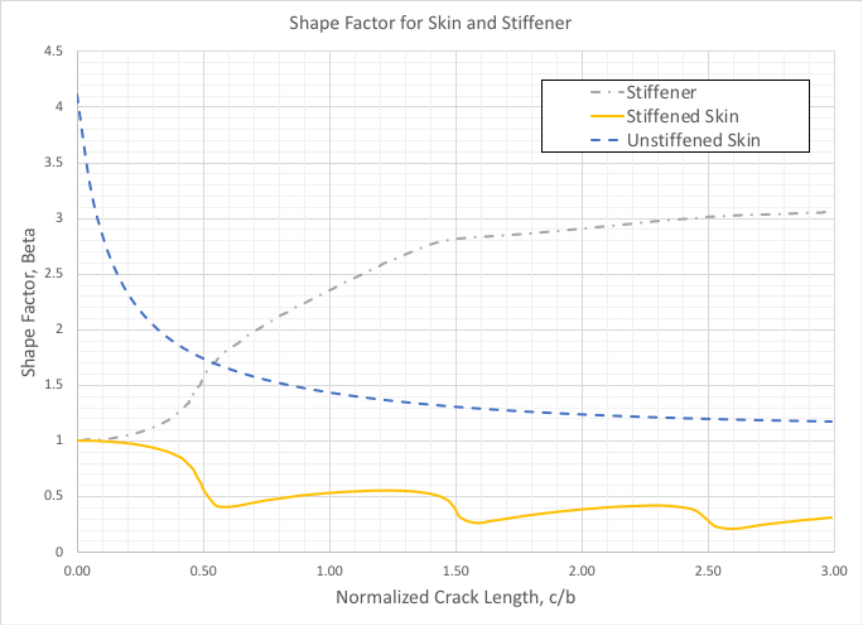

Figure 4. Shape Factor. *The figure shows the shape factor of the panel and stiffener as a function of the crack length.*

C. Plastic Stress Intensity Ratio

The plastic stress intensity ratio is the ratio of the plastic stress intensity to the elastic stress intensity. It measures the relative importance of plastic effects within the material. For some panel geometries, an analytical solution may be computed. However, this was done numerically for the present study. This was accomplished for the stiffened panel by computing eq. (1), as a function of the effective crack length, and dividing it by eq. (1) computed as a function of the original crack length. The results showed that plasticity in the material is negligible for all crack lengths, as the plastic stress intensity ratio was equal to one for all crack lengths. Figure 5 shows these results. As an additional note, calculation of eq. (3) resulted in $I = 6$ for all crack lengths, which confirmed that the panel is in a state of plane strain for all crack lengths.

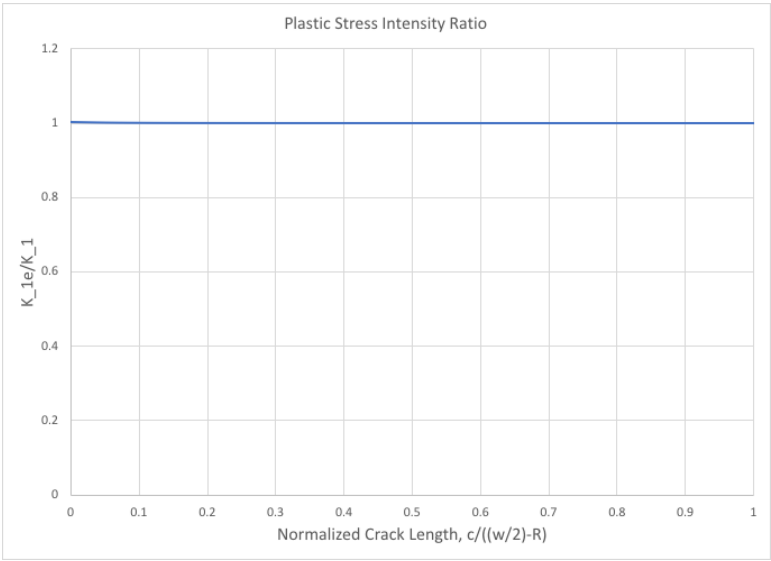

Figure 5. Plastic Stress Intensity Ratio. *The panel was in a state of plane strain for all crack lengths.*

III. Residual Strength

The residual strength of the panel is measure of panel's ability to resist further damage once a crack has started. The residual strength of the stiffened panel was calculated using three methods: brittle fracture mechanics, net-section yield, and the Fedderson approach.

A. Brittle Fracture

Residual strength is estimated through the brittle fracture method by rearranging Eq. (1) to solve for the applied stress, as shown in Eq. (13).

$$\sigma_C \quad \frac{K_{Ic}}{\sqrt{\pi c}\beta} \tag{13}$$

In order to compute Eq. (13), the fracture toughness, K_{IC}, must be known. Once this has been found, Eq. (13) may be computed over a range of crack lengths. A disadvantage of this approach is that is produces inaccurate results at short crack lengths. As the crack length approaches zero, the residual strength approaches infinity, which is an unrealistic scenario. Equation (13) is plotted in fig. 6.

B. Net-Section Yield

The net-section yield method is computed by Eq. (14). This approach produces realistic results for all crack lengths, unlike the brittle fracture approach. However, it does not account for failures due to fracture. At stress levels that do not grow cracks, this method is appropriate, but it cannot account for failure above the critical stress, σ_c. Equation (14) is plotted in fig. 6.

$$\sigma_r \quad \frac{\sigma_{YS} A_{net}}{A_{gross}} \tag{14}$$

C. Fedderson Approach

The Fedderson approach attempts to capture the best parts of the brittle fracture and net-section yield methods. This approach, which was used on the panel of interest, removes the discontinuity from the brittle fracture approach, and includes brittle fracture and net-section properties. The discontinuity is removed by drawing a tangent line from the net-section-yield y-intercept to the brittle fracture line. The benefits of the net-section yield method are then included by choosing the lower value of the two methods wherever the lines intersect. Figure 6 shows the results of the residual strength study.

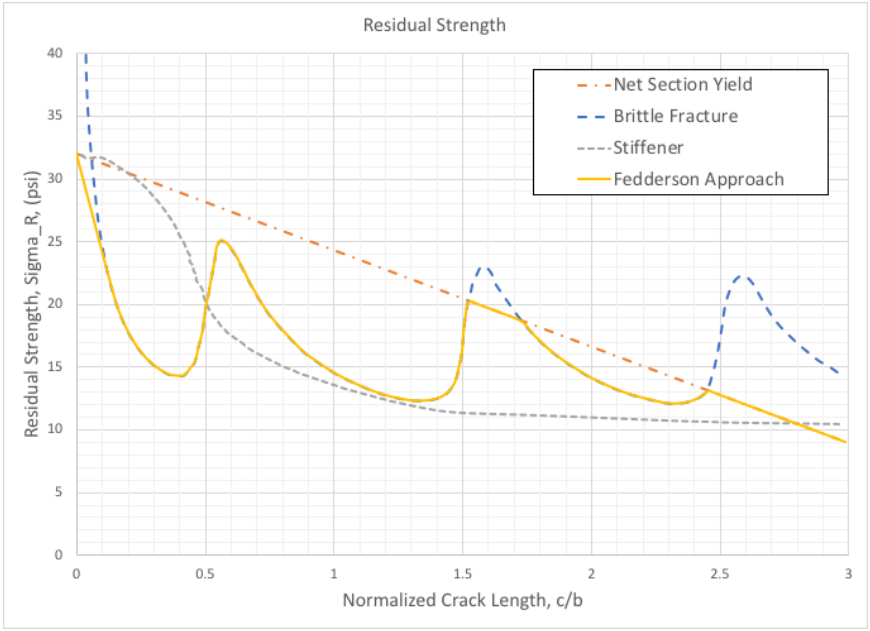

Figure 6. Residual Strength. *The residual strength of the panel is shown as a function of the normalized crack length.*

The results of the study show that there is a small range of stable crack growth. The region from c/b = 0.4 to c/b = 0.5 is the only region in which stable growth occurs. At c/b = 0.5, crack growth is arrested due to the first stiffener. However, after this point, crack growth is unstable. After c/b = 1.5, the panel generally fails due to net-section yielding.

IV. Fatigue Life

Failure is often initiated due to repeated, or cyclic, use of some part. The hanging clothes bag undergoes repeated loading over its lifespan due to the loading and unloading clothing for various travel occasions. Some occasions require more clothing than others, and thus place more stress on the internal support structure.

The fatigue life of the bag was estimated using both a stress-based and strain-based approach. The loading cycle was estimated based on the average use of an individual attending weddings throughout the year.

A. Loading Cycle

The loading spectrum for the clothes bag is shown in fig. 7. For the majority of the wedding season, the remote stress did not exceed 2 psi. However, during the peak wedding season the remote stress reached 16 psi, which is eight times the normal loading. Due to the negligible effect of plasticity found in section IIC, crack retardation was assumed to be negligible.

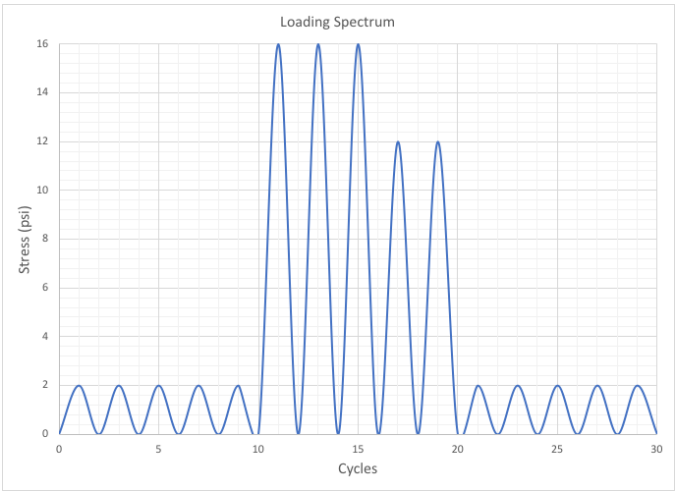

Figure 7. Loading Spectrum. *The loading occasionally increases to eight times the normal loading.*

B. Stress-based Approach

Stress-based analysis was conducted in accordance with the Palmgren-Miner rule. This rule suggests that each type of loading within a repeatable block contributes a percentage of the overall life of the part in question. Thus, equations (15) – (18) were used to calculate the number of cycles to failure for the stress-based analysis.

$$B_f \left[\sum_{j=1}^{n} \frac{N_j}{N_{fj}}\right]_{one\ rep.} \quad 1 \tag{15}$$

$$N_{fj} \quad \frac{1}{2}\left(\frac{\sigma_a}{\sigma_f' \quad \sigma_m}\right)^{\bar{b}} \tag{16}$$

$$\sigma_a \quad \frac{\sigma_{max} \quad \sigma_{min}}{2} \tag{17}$$

$$\sigma_m \quad \frac{\sigma_{max}+\sigma_{min}}{2} \tag{18}$$

Table 2 shows the results of the calculation of equations (15) – (18) as well as additional information used for the Walker-Boeing method, which is discussed in subsection C and section V.

Table 2. Palmgren-Miner Rule and Walker-Boeing Method.

j	Nj	Smin	Smax	Sa	Sm	Nfj	Nj/Nfj	R	Z	zSmax	Seff^P
1	5	0	2	1	1.5	1.38E+13	3.62E-13	0	1	2	5.66E+01
2	3	0	16	8	12	5.84E+01	5.14E-02	0	1	16	4.92E+04
3	2	0	12	6	9	7.50E+03	2.67E-04	0	1	12	1.20E+04
4	5	0	2	1	1.5	1.38E+13	3.62E-13	0	1	2	5.66E+01
Total							**5.17E-02**				**6.12E+04**

$$B_f \quad (5.17e \quad 02)^{\ 1} \quad 19\ blocks\ to\ failure$$
$$N_f \quad 15B_f \quad 285\ cycles\ to\ failure$$

Failure analysis through the Palmgren-Miner rule estimated that the support structure failed after 19 blocks, or 285 cycles, of the loading presented in fig. 7.

C. Strain-based Approach

The support structure was evaluated through the strain-based approach by computing equations (19) – (21).

$$\epsilon_a \quad \epsilon_e + \epsilon_p \tag{19}$$

$$\epsilon_e \quad \frac{\sigma_f'}{E}\left(1 \quad \frac{\sigma_m}{\sigma_f'}\right)\left(2N_f\right)^b \tag{20}$$

$$\epsilon_p \quad \epsilon_f'\left(2N_f\right)^{c_2} \tag{21}$$

However, in order to compute the cycles to failure with the strain-based approach, a single loading spectrum, equivalent to the spectrum shown in fig. 7, was required. It was important, however, that the loading spectrums be equivalent from the standpoint of crack growth. This means that the two spectrums should cause a particular crack to grow the same amount, despite the loadings being of different magnitudes or frequency. The equivalent load spectrum of the block shown in fig. 7 was computed using the Walker-Boeing method, which is shown in Eq. (22), and resulted in an equivalent block load of $S \quad 23.3\ psi$, as shown in fig. 9. Some of the results of equations (22) – (24) are shown in the four columns on the right of Table 2 from the previous subsection.

$$\sum_{j=1}^{n}(z\sigma_{max})_j^p N_j \quad S^p \tag{22}$$

$$Z \quad (1 \quad R_2)^q \tag{23}$$

$$R_2 \quad \frac{\sigma_{min}}{\sigma_{max}} \tag{24}$$

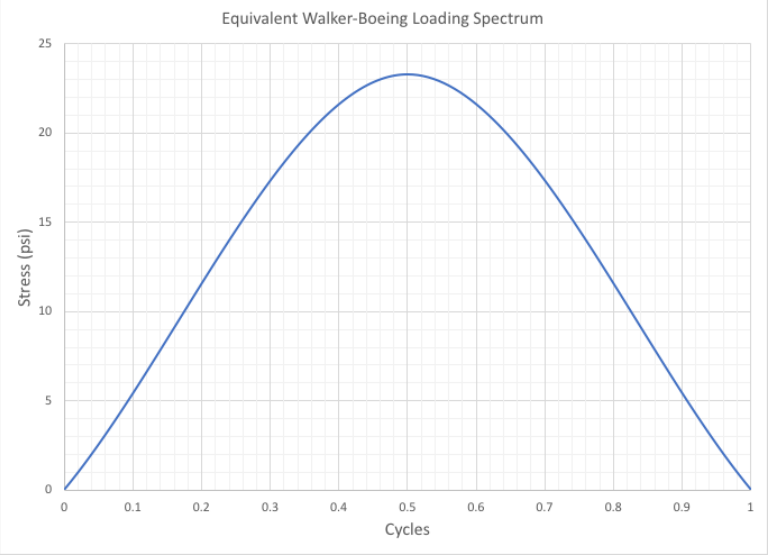

Figure 8. Walker-Boeing Equivalent Load. *The graph shows the equivalent single-block load as compared to the loading spectrum in fig. 7.*

After computing the equivalent load, *S*, the equivalent strain amplitude was computed through Eq. (25).

$$\epsilon_a \quad S/E \tag{25}$$

Equation (19) was then set equal to Eq. (25), after which the cycles to failure, N_f, was computed numerically. The strain-based approach predicted failure at N_f = 300 cycles (20 blocks), which is in close agreement with the stress-based approach.

Additionally, evaluation of Eq. (19) over a range of cycles resulted in fig. 8, shown to the right. Figure 8 shows the components of the strain amplitude as a function of cycles. An important point in fig. 8 is the location of the transition cycle, N_T. The transition cycle is the point where the relative importance of the elastic and plastic strains changes. They are numerically equal at this point as well. At lower cycles, plastic strain is more influential, whereas at higher cycles, elastic strain is more influential. Additionally, strain-based analysis is typically more appropriate below this point, whereas stress-based analysis is more appropriate above it.

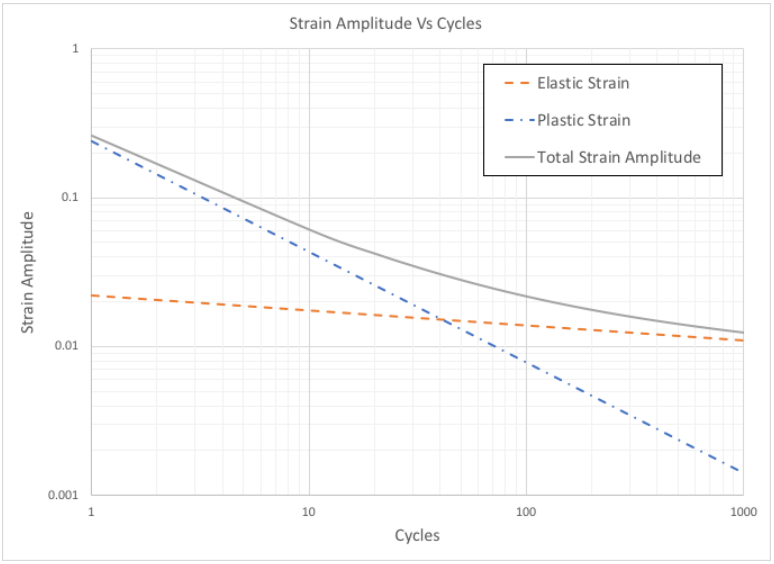

Figure 9. Strain Amplitude. *The transition from plastic strain to elastic strain occurs near N_T = 41 cycles.*

In the case of the present study, it was determined in section IIC that plasticity was negligible, as the inclusion of plastic effects in Eq. (1) produced the same results as when they were not included. As such, it was expected that the failure cycle would be within the elastic strain region. Therefore, by setting eq. (20) equal to eq. (21), the transition cycle was found to be N_T = 41 cycles, which is below the failure cycle predicted by both the stress-based and strain-based approaches. This showed the assumption of negligible plasticity to be valid.

V. Crack Propagation

Once a crack develops, it is important to know the rate at which it will grow, given a certain loading. Two methods were used in the present study to estimate the crack propagation in the present study: the Paris law and the Walker-Boeing method.

A. Critical Crack Length

The first step in estimating crack propagation is the determination of the minimum inspectable crack length and the critical length at which the part will ultimately fail. Section IV was concerned with the number of cycles until the development of an inspectable crack, but not necessarily the ultimate failure of the panel. The critical crack length, therefore, corresponds with ultimate panel failure.

The minimum inspectable crack length, c_0, was determined to be c_0 0.1 in, through visual inspection. In order to determine the critical crack length, c_f, Eq. (1) was re-arranged to solve for the crack length, while substituting the panel fracture toughness, K_{IC}, for the stress intensity and substituting the Walker-Boeing equivalent stress, *S*, for the applied stress. This resulted in a critical crack length of c_f 0.3 in.

B. Paris Law

Once the crack limits were determined, the number of cycles to grow the crack between the limits was determined through integration of the Paris law, shown in equations (26) – (27).

$$\frac{da}{dN} \quad C(\Delta K)^n \quad C(K_{max} \quad K_{min})^n \tag{26}$$

$$N_f \quad \frac{1}{C(S\sqrt{\pi})^n} \int_{a_0}^{a_f} a^{\,n/2} \beta^{\,n} da \tag{27}$$

Evaluation of Eq. (26) over zone II of the crack range produced fig. 10, shown below. Since the form factor, β, is a function of the crack length, Eq. (27) was integrated numerically in MATLAB using the trapezoidal rule of numerical quadrature. Evaluation of Eq. (27) resulted in $N_f = 0$ *cycles.* This means that once an inspectable crack is detected, any further loading of the support structure will cause immediate failure.

C. Walker – Boeing Method

The Walker-Boeing Method is defined by Eq. (28). Similar to the Paris law in the previous subsection, this method was re-arranged and integrated numerically, as shown in Eq. (29).

$$\frac{da}{dN} \quad \frac{10^{-4}(ZK_{max})^p}{m_T^p} \tag{28}$$

$$N_f \quad \frac{m_T^p}{10^{-4}(S\sqrt{\pi})^p} \int_{a_0}^{a_f} a^{\,p/2} \beta^{\,p} da \tag{29}$$

Evaluation of Eq. (29) resulted in $N_f = 0$ *cycles*, which agrees with the estimate provided by the Paris law.

Additionally, Eq. (28) was also plotted over the zone II range of crack growth. Figure 10 shows that when K_{max} is equal to K_c 6 $psi\sqrt{in}$, the Paris law predicts a crack growth rate of da/dN 0.7 $in/cycle$ and the Walker-Boeing method predicts a growth rate of da/dN 0.3 $in/cycle$. These results agree with the results of the integration that additional cycles after the initial crack is detected could result in complete failure of the structure. Since the difference between the critical crack length and the initial crack length is 0.2 inches, the Paris law and the Walker-Boeing method predict failure in less than one complete cycle. This essentially means that failure occurs immediately.

Figure 10. Crack Growth Rate. *The chart shows the predicted zone II crack growth rates of both the Paris Law and the Walker-Boeing Method.*

VI. Inspection Cycle

Proper inspection cycles over the life of a hanging clothes bag can ensure years of reliable use and potentially help to avoid adding wrinkles to one's clothing. In section IV it was determined that the structure would develop an inspectable crack after approximately 300 cycles. The crack propagation analysis of section V determined that any further loading of the bag would result in immediate failure of the structure. Due to this, an initial inspection should be accomplished at 250 cycles. The support structure should be inspected every cycle thereafter, to ensure that any

cracks are discovered. To ensure that no clothing experiences wrinkling due to the failure of the support structure, the structure should be replaced when a crack is detected, but no later than 290 cycles.

VII. Design Improvements

The design of the support structure could be improved in several ways to ensure better performance over its lifetime. The options include, but are not limited to, the following:

- Use a stronger material
- Increase the thickness of the panel
- Increase the amount stiffeners
- Change the design to a single, thick panel, rather than a stiffened, thin panel

The first two suggestions are evaluated below. The new material is Aluminum 2024-T351 and the panel thickness has been increased from 0.03125 *in* to 0.0625 *in.*

A. Stress Intensity

The stress intensity of the improved panel was evaluated in the same manner as section II. The results of this evaluation remained the same as before, with plasticity being negligible.

B. Residual Strength

Significant differences were observed in the residual strength of the new panel as compared to the original panel. In addition to the critical strength being approximately 1700 times higher, the improved panel would not fail due to fracture. Rather, the improved panel would fail first due to net-section yielding.

Additionally, in this case, the Fedderson approach to the analysis would yield the same line as the net-section yield approach, since it is lower than the brittle fracture line. Figure 11 shows the residual strength of the improved panel.

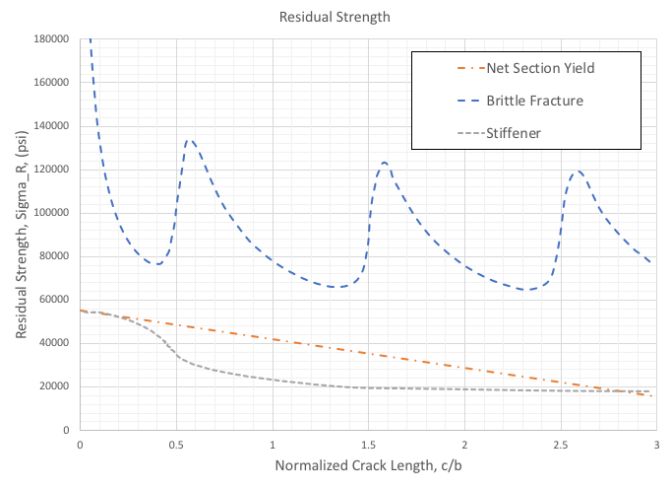

Figure 11. Residual Strength of the Improved Panel. *The Fedderson approach for the improved panel is equivalent to the Net-Section Yield line.*

C. Fatigue Life

The improved panel performed significantly better in tests for fatigue life as well. Following the same procedures previously described, the fatigue results are as follows:

- Stress-based approach:
  - N_f = 3.8e36 blocks
  - N_f = 5.7e37 cycles to failure
- Strain-based approach:
  - N_f = 9e35 blocks
  - N_f = 1.35e37 cycles to failure
- Transition cycle: N_T = 161 cycles

Again, there is close agreement between the stress-based and strain-based approaches. However, since the endurance limit for aluminum alloys is approximately 10^8 cycles, the improved panel will not fail due to fatigue, as it is not under enough stress. The aluminum panel is also subjected to less strain. The improved strain amplitude is shown in fig. 12.

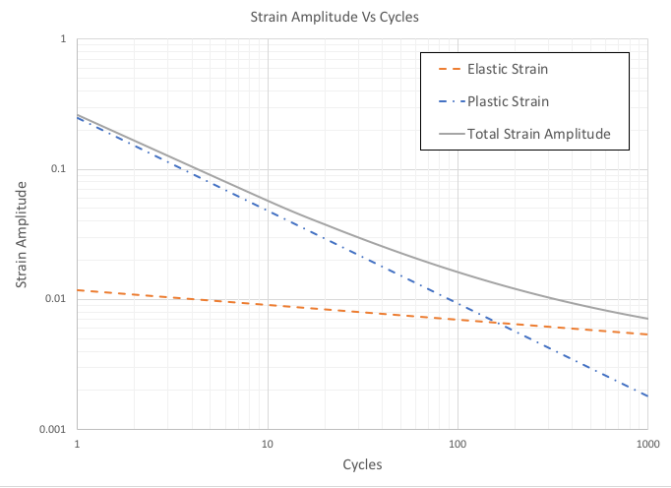

Figure 12. Improved Strain Amplitude. *The improved material properties reduced the strain.*

D. Crack Propagation

Crack propagation analysis was omitted for the new panel since the residual-strength analysis and fatigue-life analysis both showed that the improved panel cannot fail due to cracking at the applied load. The residual-strength analysis showed that, if failure were to occur, the failure would be due to net-section yielding. Additionally, the fatigue-life analysis showed that the applied stress is far below the endurance limit of the material.

VIII. Conclusion

Hanging clothes bags can be an important part of an individual's wardrobe as they can protect clothes from becoming wrinkled while traveling. When the internal support structure of these bags fails, it is important to thoroughly investigate the cause. The failure investigation of the student's clothes bag included stress intensity, residual strength, fatigue life, and crack propagation. Additionally, inspection intervals and possible damage-tolerant improvements were suggested.

The study of the stress intensity determined that both the original panel and the improved panel were in a state of plain strain for all crack lengths studied. The presence of the stiffeners also greatly reduced the stress intensity relative to an unstiffened, reference panel.

Analysis of the residual strength produced very different results between the two panels. The original panel failed due to a combination of brittle fracture and net-section yielding. The panel failed due to brittle fracture at short crack lengths, whereas it failed due to net-section yielding after reaching crack lengths of approximately $c = 1/32$ inch. The improved panel, however, could only fail due to net-section yielding if the loading was greatly increased.

Test for fatigue life also showed drastically different properties between the panels. The original panel failed near 300 cycles, whereas the improved panel did not fail due to fatigue. This was because the applied stress was below the endurance limit for the material.

The crack propagation analysis showed that cracks in the original panel would grow to the critical crack length immediately following the initial development of a crack. Crack propagation analysis was not conducted for the improved panel, since the residual-strength and fatigue-life test determined that the panel could not fail due to fracture.

Without changing the design of the support structure, inspection cycles were recommended as a means of preventing failure of the structure. It was recommended that an initial inspection be accomplished after 250 cycles, and every cycle thereafter. The structure should be replaced as soon as a crack develops or at 290 cycles, whichever is first.

Finally, it was shown that changing the material to Aluminum 2024-T351 and increasing the panel thickness to 1/16 *in* can greatly improve the life of the hanging clothes bag. These improvements greatly reduce the possibility of important clothing becoming wrinkled while traveling.

References

[1] Smith, Bert L., Horn, Walter J., Failure, Fracture Mechanics, Fatigue, and Damage Tolerance, 1st ed., Wichita State University.